Rovibronic bands of the A B 2 2 X B 2 1 transition of C 6 H 5 O and C 6 D 5 O detected with cavity ringdown absorption near 1.2 m

Chi-Wen Cheng, Henryk Witek, and Yuan-Pern Lee

Citation: The Journal of Chemical Physics **129**, 154307 (2008); doi: 10.1063/1.2992077
View online: http://dx.doi.org/10.1063/1.2992077
View Table of Contents: http://scitation.aip.org/content/aip/journal/jcp/129/15?ver=pdfcov
Published by the AIP Publishing

Rovibronic bands of the $\tilde{A}\,^2B_2 \leftarrow \tilde{X}\,^2B_1$ transition of C_6H_5O and C_6D_5O detected with cavity ringdown absorption near 1.2 μm

Chi-Wen Cheng,[1] Henryk Witek,[1] and Yuan-Pern Lee[1,2,a)]
[1]*Department of Applied Chemistry and Institute of Molecular Science, National Chiao Tung University, 1001, Ta-Hsueh Rd., Hsinchu 30010, Taiwan*
[2]*Institute of Atomic and Molecular Sciences, Academia Sinica, Taipei 10617, Taiwan*

(Received 26 June 2008; accepted 8 September 2008; published online 17 October 2008)

We recorded several rovibronic bands of C_6H_5O and C_6D_5O in their $\tilde{A}\,^2B_2 \leftarrow \tilde{X}\,^2B_1$ transitions in the range 1.14–1.31 μm with the cavity ringdown technique. While the electronic transition is forbidden, several vibronic bands are observed. By comparison of rovibronic contours of observed and simulated bands to determine their types of transition, and by consideration of vibrational wavenumbers of the upper state based on quantum-chemical calculations, we were able to provide vibronic assignments of observed bands and derive several experimental vibrational wavenumbers (given as ν in unit of cm^{-1} in this paper) for the $\tilde{A}\,^2B_2$ state, namely, ν_{12}=947, ν_{13}=793, ν_{14}=417, ν_{15}=964, ν_{16}=866, ν_{17}=723, ν_{18}=680, and ν_{19}=499 for C_6H_5O, and ν_{12}=772, ν_{13}=626, ν_{14}=365, ν_{15}=812, ν_{17}=599, ν_{18}=532, and ν_{19}=436 for C_6D_5O. Transitions involving vibrationally excited levels of ν_{20} were also observed; ν_{20} of the $\tilde{A}$ state is greater by 50 cm^{-1} than the $\tilde{X}$ state of C_6H_5O. A weak origin at 7681 cm^{-1} for the $\tilde{A} \leftarrow \tilde{X}$ transition of C_6H_5O (7661 cm^{-1} for C_6D_5O) with a *c*-type contour was observed. Observed isotopic ratios of vibrational wavenumbers for the $\tilde{A}$ state of C_6H_5O to those of C_6D_5O are in good agreement with the predictions from quantum-chemical calculations at the B3LYP/aug-cc-pVTZ level. © *2008 American Institute of Physics*. [DOI: 10.1063/1.2992077]

I. INTRODUCTION

The phenoxy (C_6H_5O) radical is an important intermediate in the oxidation of small aromatic compounds that are important constituents of fuels.[1–4] Kinetics for reactions of C_6H_5O with O_2, O_3, NO, NO_2, and CH_3 have been investigated in detail.[5–9] Most investigations on kinetics of gaseous C_6H_5O utilized broad electronic absorption bands of C_6H_5O in the UV or visible region. Popular methods for production of C_6H_5O include laser or flash photolysis of phenol (C_6H_5OH) or anisol ($C_6H_5OCH_3$).

C_6H_5O has a ground electronic state designated as $\tilde{X}\,^2B_1$. The C–O bond was indicated to have a double-bond character, based on the results of electron spin resonance (ESR) spectroscopy.[10–15] Several vibrational modes of C_6H_5O were identified with resonance-enhanced Raman spectroscopy,[16–20] but most vibration fundamentals of C_6H_5O remained unknown. The infrared analysis of gaseous C_6H_5O is unreported, only matrix-isolated C_6H_5O, produced upon photolysis of nitrobenzene or nitrosobenzene at 308 nm, has been reported; 26 of the 30 fundamental vibrational modes were identified.[21]

Electronically excited states of $\tilde{B}\,^2A_2$, $\tilde{C}\,^2B_1$, $\tilde{D}\,^2A_1$, and $\tilde{E}\,^2B_1$ have been characterized with absorption bands in regions of 510–640 nm,[8,21–26] 370–400 nm,[9,21,22,25–27] 270–300 nm,[5,6,21,23,25,27–29] and 220–250 nm,[5,6,25,29] respectively. Only the $\tilde{B}\,^2A_2 \leftarrow \tilde{X}\,^2B_1$ transition shows a resolved vibrational progression of spacing ~480 cm^{-1}.[24,25]

The $\tilde{A}\,^2B_2 \leftarrow \tilde{X}\,^2B_1$ transition of C_6H_5O is symmetry forbidden but vibronically allowed. The weakness of this transition has precluded detailed investigation of the $\tilde{A}\,^2B_2$ state. Gunion *et al.*[30] observed a band near 1170 nm (8550 cm^{-1}) in the photoelectron spectrum upon photodetachment of gaseous $C_6H_5O^-$ and assigned it as the $\tilde{A} \leftarrow \tilde{X}$ transition of C_6H_5O. Radziszewski *et al.*[25] employed ultraviolet-visible polarization absorption spectroscopy and determined directions of transition dipole for several low-lying electronic states of C_6H_5O isolated in solid Ar. They reported an extremely weak band near 1123 nm (8900 cm^{-1}) with undetermined direction of the transition dipole and assigned it as the $\tilde{A} \leftarrow \tilde{X}$ transition. If the observed bands in these experiments are associated with the same transition, the blueshift of 350 cm^{-1} for matrix-isolated C_6H_5O seems to be uncommon.

Most theoretical calculations on the ground electronic state of C_6H_5O indicate that C_6H_5O is planar with a $\tilde{X}\,^2B_1$ ground state.[21,31–34] The predicted bond length of C–O is ~1.24 Å, closer to the length of a CO double bond of 1.215 Å for acetone than that of a CO single bond of 1.364 Å for phenol,[35] consistent with the results from ESR. To our knowledge, quantum-chemical calculations on only vertical excitations but not on the adiabatic excitation energy of electronic excited states of C_6H_5O are reported. The reported vertical excitation energy of the $\tilde{A}\,^2B_2$ state varied

a)Author to whom correspondence should be addressed. Electronic mail: yplee@mail.nctu.edu.tw.

from 5322 to 12685 cm^{-1}.[9,25,33,34,24,36–40] The predicted CO bond length of C_6H_5O increases from ~1.24 Å in its ground state to ~1.35 Å in its $\tilde{A}\,^2B_2$ state, indicating a single-bond character for the $\tilde{A}$ state.

We have recently successfully employed the cavity ringdown technique near the 1.2–1.4 μm region to investigate weak rovibronic bands of gaseous CH_3OO and CD_3OO in their $\tilde{A}\leftarrow\tilde{X}$ transitions and reported several vibrational frequencies of the $\tilde{A}$ state.[41] The high sensitivity of the cavity ringdown technique is suitable to investigate electronically forbidden transitions of free radicals. We report here the first observation of the $\tilde{A}\,^2B_2\leftarrow\tilde{X}\,^2B_1$ vibronic system and identification of several vibrational wavenumbers of the $\tilde{A}\,^2B_2$ state of C_6H_5O using the cavity ringdown technique.

II. EXPERIMENTS

The principles and techniques of cavity ringdown have been discussed extensively.[42] For absorption spectra based on cavity ringdown one measures the decay of intensity of a laser pulse trapped in an optical cavity formed between two highly reflective mirrors.[41,43] When the cavity contains an absorbing medium, which for these experiments is C_6H_5O or C_6D_5O, the ringdown period is decreased at those wavelengths at which absorption occurs. The ringdown period τ is defined as the temporal interval required for the intensity to decay to $1/e$ of its initial value. In the presence of an absorbing species the ringdown period τ' becomes

$$\tau' = L/[c(1-R+\alpha l)], \tag{1}$$

in which c is the speed of light, R is the reflectivity of the mirror, l is the path length (in cm) of the absorbing medium, L is the length of the cavity, and $\alpha=\sigma N$ is the absorption coefficient, in which σ is the cross section of absorption in cm^2, and N is the number density of absorbing molecules in cm^{-3}. The absorption per unit length is hence simply related to the difference in cavity ringdown periods of τ' determined when the absorption species was present and τ when the absorption species was absent,

$$\alpha = \left(\frac{1}{\tau'}-\frac{1}{\tau}\right)\frac{L}{cl}. \tag{2}$$

The laser radiation employed for cavity ringdown was generated by shifting the output of a dye laser (Spectra Physics, Model Sirah, with a mixture of exciton dyes LDS 867, LDS 821, and LDS 765) with a single-pass Raman shifter employing gaseous H_2 at ~15 bars to produce emission near 1.2 μm with energy ~1 mJ $pulse^{-1}$. The dye laser was pumped with a Nd:YAG (yttrium aluminum garnet) laser (Spectra Physics, PRO-270, 10 Hz) to generate output of 20–40 mJ in the range 765–860 nm. The spectral width of this laser system is ~0.06 cm^{-1} and the wavelength scanning steps were 0.05 nm (~0.7 cm^{-1}). The ringdown signal was recorded with an InSb detector (Kolmar, KISDP-1-LJ2, rise time of 520 ns) cooled to 77 K. The signal was amplified (1 MHz bandwidth) and recorded with a digital computer oscilloscope (14 bits, Gage Applied Technologies, Compuscope 14100), and subsequently processed with a personal computer. Typically the waveform was averaged over 30 laser pulses at each wavelength. We calibrated the wavelength of the dye laser with a wavemeter (Burleigh, 4500) and the lines of the $\tilde{a}\,^1\Delta_g\leftarrow\tilde{X}\,^3\Sigma_g^-$ system of molecular oxygen according to the HITRAN database.[44] The accuracy of measurements of wavelength is estimated to be ±0.012 nm.

A flowing system was employed to achieve steady-state conditions of C_6H_5O. The flow reactor has two rectangular (2.5×15 cm^2) quartz (S1UV) plates on the side for photolysis. The length of the cavity, formed between two highly reflective mirrors (Los Gatos Research, $R\cong0.999\,95$ near 1.2 μm and $R\cong0.9999$ near 1.3 μm), is 63 cm. The cavity mirrors were purged with N_2 to avoid possible damage by the reactants. C_6H_5O was produced by photolysis of anisol ($C_6H_5OCH_3$, Aldrich, 99%) or phenetole ($C_6H_5OC_2H_5$, Aldrich, 99%) at 193 nm (Lambda Physik, LPX110i, 10 Hz, 45 mJ). The total pressure of the system was typically 220 Torr with $C_6H_5OCH_3:N_2\cong1:72$. C_6D_5O was produced from fully deuterated anisol (Aldrich, 98%).

III. THEORETICAL CALCULATIONS

Detailed calculations on the geometry, energy, and vibrational frequencies of C_6H_5O and C_6D_5O in their electronic ground and first excited states have been reported previously.[31] The geometry and energy of C_6H_5O in its $\tilde{A}$ and $\tilde{X}$ states were calculated with unrestricted hybrid density functional method (B3LYP), complete active space self-consistent-field (CASSCF), and complete active space second-order perturbation theory (CASPT2) methods; nine active electrons distributed among eight orbitals, designated as (9,8), were used for the latter two methods. Various basis sets were tested; predicted vibrational wavenumbers and electronic excitation energy show little dependence on the basis sets. We employ results using the aug-cc-pVTZ basis set for comparison with experiments.

The ground electronic state of C_6H_5O has a C_{2v} symmetry; we define the molecular plane as the yz plane and the direction of the CO bond as the z-axis. The rotational a-, b-, and c-axis coincide with the z-, y-, and x-axis, respectively. Rotational constants of the $\tilde{A}$ and $\tilde{X}$ states based on the predicted geometries are listed in Table I; these values vary less than 1.6% between various basis sets and methods. The results from B3LYP/aug-cc-pVTZ are used in the spectral simulation.

Related molecular orbitals of the $\tilde{A}$ and $\tilde{X}$ states of C_6H_5O are shown in Fig. 1; SOMO indicates the singly occupied molecular orbital, HOMO indicates the highest doubly occupied molecular orbital, and HOMO$-n$ indicates the nth lower doubly occupied molecular orbital. The transition $\tilde{A}\,^2B_2\leftarrow\tilde{X}\,^2B_1$ involves excitation of an electron from the third highest doubly occupied molecular orbital (HOMO−2) to the SOMO. In the ground electronic state, orbitals of the O atom are extensively involved with bonding of the benzene ring. The HOMO−2 involves approximately a nonbonding orbital of O atom, whereas the SOMO has a π^* character for the O atom and the benzene ring. Upon the $\tilde{A}\leftarrow\tilde{X}$ transition, the latter orbital becomes doubly occupied and changes its

TABLE I. Rotational constants A, B, and C (in cm^{-1}) of the $\tilde{X}$ and $\tilde{A}$ states of C_6H_5O and C_6D_5O calculated with various methods.

Molecule	State	Rotational constant	B3LYP /aug-cc-pVTZ	B3LYP /aug-cc-pVDZ	CASSCF /aug-cc-pVDZ
C_6H_5O	$\tilde{X}$	A''	0.184 9	0.182 8	0.182 0
		B''	0.093 39	0.092 43	0.093 28
		C''	0.062 05	0.061 39	0.061 67
	$\tilde{A}$	A'	0.190 4	0.188 1	0.188 6
		B'	0.092 46	0.091 55	0.091 55
		C'	0.062 24	0.061 57	0.061 63
C_6D_5O	$\tilde{X}$	A''	0.153 4	0.151 7	0.151 2
		B''	0.086 10	0.085 18	0.085 97
		C''	0.055 00	0.054 55	0.054 80
	$\tilde{A}$	A'	0.157 5	0.155 5	0.156 1
		B'	0.085 30	0.084 47	0.084 50
		C'	0.055 35	0.054 74	0.054 83

nature and energy substantially, as shown in Fig. 1. The approximate $n \rightarrow \pi^*$ excitation implies that the CO bond length of the $\tilde{X}$ state (1.26 Å) becomes greater in the $\tilde{A}$ state (1.32 Å). The bond lengths of C1-C2 and C2-C3 in the $\tilde{X}$ state vary from 1.46 to 1.38 Å, whereas those in the $\tilde{A}$ state are similar (1.41 and 1.39 Å); the equilibrium ring structure of the $\tilde{A}$ state of C_6H_5O is similar to that of benzene in its ground electronic state.

Previous calculations provided only vertical excitation energy with values ranging from 5322 to 12 685 cm^{-1}. The vertical and adiabatic excitation energies of the $\tilde{A} \leftarrow \tilde{X}$ transition calculated with B3LYP/aug-cc-pVTZ, CASSCF(9,8)/aug-cc-pVTZ, and CASPT2(9,8)/aug-cc-pVTZ methods are compared with previous results in Table II. The adiabatic excitation energy (zero-point energy corrected), with values 7242, 6694, and 8339 cm^{-1} from B3LYP/aug-cc-pVTZ, CASSCF(9,8)/aug-cc-pVTZ, and CASPT2(9,8)/aug-cc-pVTZ, respectively, are all smaller than the energy of the observed band at 8550 or 8900 cm^{-1}.[25,30]

Scaled harmonic vibrational wavenumbers of C_6H_5O and C_6D_5O in their $\tilde{A}$ state predicted with the B3LYP/aug-cc-pVTZ method are compared with experimental results in Table III; the ordering of vibrational modes follows that of Herzberg.[45] The vibrational wavenumbers scaled by single scaling factors of 0.967 and 0.970 for C_6H_5O and C_6D_5O, respectively, are listed in Table III; the scaling factors were derived by comparison of calculated and experimental values of phenol.[31] The predicted vibrational wavenumbers of the $\tilde{X}$ state (not listed) are similar to those reported previously for C_6H_5O and C_6D_5O isolated in solid Ar;[21] the deviations are less than 8% and 6%, respectively.

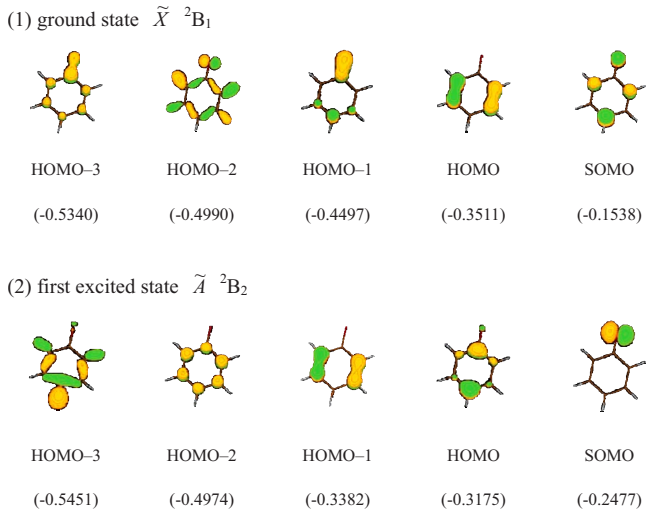

FIG. 1. (Color online) The first few highly occupied molecular orbitals (HOMOs) and singly occupied molecular orbitals (SOMOs) of C_6H_5O in their $\tilde{A}$ and $\tilde{X}$ states predicted with CASSCF(9,8)/cc-pVDZ. The energies in hartree are listed in parentheses. See details in the Supporting Information (Table K) of Ref. 31.

IV. EXPERIMENTAL RESULTS AND DISCUSSION

A. Vibronic bands of C_6H_5O

Upper traces in panels (A)–(D) of Fig. 2 present observed spectra in the region 7660–8760 cm^{-1} (1.14–1.31 μm) upon photolysis of a flowing mixture of

TABLE II. Adiabatic and vertical excitation energies of the $\tilde{A} \leftarrow \tilde{X}$ transition of C_6H_5O derived with various methods.

Method	Adiabatic (cm^{-1})	Vertical (cm^{-1})	Ref.
Cavity ringdown	7681		This work
Matrix isolation	8900		25
Photoelectron	8550		30
CNDO		5 322	36
TD-B3LYP/aug-cc-pVTZ		~8 400	9, 25, and 40
CASSCF(9,8)/6-31G*		10 564	34
MRSDCI		12 685	33
B3LYP/aug-cc-pVTZ	7242	8 548	31
B3LYP/aug-cc-pVDZ	7323	8 605	31
CASSCF(9,8)/aug-cc-pVTZ	6694	10 927	31
CASPT2(9,8)/aug-cc-pVTZ	8339	9 952	31

TABLE III. Comparison of scaled harmonic vibrational wavenumbers (in cm^{-1}) of C_6H_5O and C_6D_5O in their $\tilde{A}$ states calculated with various methods.

		C_6H_5O			C_6D_5O		
Mode	Sym.	Calc.[a]	Calc.[b]	This work	Calc.[a]	Calc.[b]	This work
ν_1	a_1	3100	3107		2306	2312	
ν_2	a_1	3091	3098		2295	2301	
ν_3	a_1	3062	3070		2266	2272	
ν_4	a_1	1556	1556		1521	1525	
ν_5	a_1	1410	1393		1274	1269	
ν_6	a_1	1202	1201		1183	1179	
ν_7	a_1	1152	1143		930	922	
ν_8	a_1	1011	1008		862	853	
ν_9	a_1	961	953		824	816	
ν_{10}	a_1	802	797		744	738	
ν_{11}	a_1	505	501		495	491	
ν_{12}	a_2	941	928	947 ± 2	768	758	772 ± 2
ν_{13}	a_2	799	787	793 ± 6	624	615	626 ± 3
ν_{14}	a_2	416	414	417 ± 2	364	361	365 ± 2
ν_{15}	b_1	955	943	964 ± 5	804	799	812 ± 7
ν_{16}	b_1	861	847	866 ± 3	726	716	
ν_{17}	b_1	710	697	723 ± 2	585	576	599 ± 2
ν_{18}	b_1	673	674	680 ± 2	544	539	532 ± 2
ν_{19}	b_1	496	490	499 ± 5	429	424	436 ± 5
ν_{20}	b_1	219	218		208	206	
ν_{21}	b_2	3099	3106		2301	2307	
ν_{22}	b_2	3067	3075		2273	2279	
ν_{23}	b_2	1529	1529		1493	1498	
ν_{24}	b_2	1408	1395		1312	1314	
ν_{25}	b_2	1304	1291		1218	1228	
ν_{26}	b_2	1222	1232		1014	996	
ν_{27}	b_2	1139	1130		829	820	
ν_{28}	b_2	1058	1052		809	801	
ν_{29}	b_2	604	599		581	576	
ν_{30}	b_2	358	354		346	343	

[a]Scaled vibrational wavenumbers calculated with B3LYP/aug-cc-pVTZ. See text and Ref. 31.
[b]Scaled vibrational wavenumbers calculated with B3LYP/aug-cc-pVDZ. See text and Ref. 31.

$C_6H_5OCH_3/N_2$ (1/72, 220 Torr). These figures represent difference spectra between those recorded before laser irradiation and 2 μs after laser irradiation at 193 nm; the scan steps are 0.05 nm. Similar spectra were recorded when a flowing mixture of $C_6H_5OC_2H_5/N_2$ (1/145, 220 Torr) was used; observed ratio of signal to noise was smaller with this precursor, so we used data from photolysis of $C_6H_5OCH_3$ for discussion. Because identical spectra were recorded from both precursors, the carrier of the spectrum should be resulted from C_6H_5, C_6H_5O, or their reaction products; the latter is less likely because the intensity of the spectrum was the greatest at near-zero delay after photolysis and decreases slightly at longer delays. According to experimental observations[46] and theoretical calculations,[47] there is no electronic state of C_6H_5 near the 1240 nm ($\sim$8066 cm^{-1}) region; the most likely carrier of the observed spectrum is thus C_6H_5O.

The $\tilde{A}\ ^2B_2 \leftarrow \tilde{X}\ ^2B_1$ transition is electronically forbidden, but some vibronic transitions are allowed due to the Herzberg–Teller effect.[48] Vibrationally excited states of the $\tilde{A}\ ^2B_2$ state with a_2, b_1, and b_2 symmetries may be directly excited from the ground vibronic state $\tilde{X}\ ^2B_1$, showing *a*-, *b*-, and *c*-type rotational contours, respectively, but modes with a_1 symmetry are forbidden. Rotational contours of the *a*-, *b*-, and *c*-type bands simulated with the PGOPHER program[49] show distinct band shapes, as indicated in Fig. 2. The *a*-type band shows *P* and *R* branches of approximate equal intensity, whereas the *b*-type band shows a prominent *Q* branch overlapped with the *P* branch; the *c*-type band reveals only narrow *Q* branches. By comparison of the observed band contours with simulations, the band type may be assigned readily. Observed bands were fitted with calculated rotational parameters predicted with B3LYP/aug-cc-pVTZ (Table I), $J_{max}=200$, $T=330$ K, and spectral width=1.0 cm^{-1} (full width at half maximum for Gaussian functions) to derive the band origins, as listed in Table IV. The spectral width is comparable to the step size (0.05 nm) of laser scanning.

Because the band origin of the $\tilde{A} \leftarrow \tilde{X}$ transition of C_6H_5O is expected to be missing due to its symmetry-forbidden nature, and because the electronic transition energy calculated quantum chemically is not accurate enough to predict the exact position of vibronic bands, it is difficult to assign these bands by direct comparison of band positions between experiments and calculations. However, we can

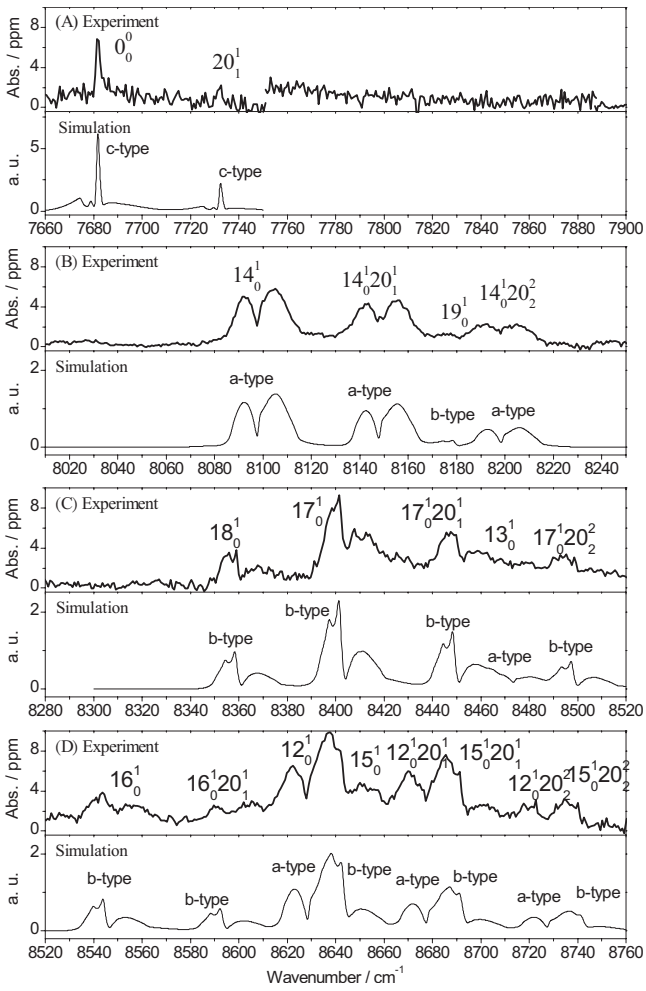

FIG. 2. Comparison of experimental spectra and simulated spectra of C_6H_5O in the region 7660–8760 cm^{-1}. The notation of the assignments is described in the text.

identify the band type by its rotational contour to provide additional information. There are only three and six vibrational modes of C_6H_5O with a_2 and b_1 symmetries, respectively. By positive identification of some *a*-type bands characteristic of the a_2 vibrational modes and *b*-type bands characteristic of the b_1 vibrational modes of C_6H_5O, vibronic assignments are possible.

For the three *a*-type bands in the region 8080–8220 cm^{-1} [Fig. 2(B)], the spacing of 50 cm^{-1} does not correspond to differences among predicted vibrational wavenumbers, 941, 799, and 416 cm^{-1}(after scaling, Table III), for the three vibrational modes of the $\tilde{A}$ state with a_2 symmetry. The separation of ~50 cm^{-1} agrees satisfactorily with the energy difference of 38 cm^{-1} between the vibrational modes of the $\tilde{A}$ state (ν_{20}=219 cm^{-1}) and the $\tilde{X}$ state (ν_{20}=181 cm^{-1}) with the least energy. The observed relative intensities of 1.00:0.54:0.14 for these three bands also agree satisfactorily with a Boltzmann distribution at 298 K for levels with energy separation ~200±70 cm^{-1}. Hence, we tentatively assigned bands near 8148±1 and 8199±2 cm^{-1} as hot bands involving one and two vibrational quanta of ν_{20}, whereas the band near 8098±1 cm^{-1} is a pure vibronic transition from the ground level of the $\tilde{X}$ state. Similar hot bands

TABLE IV. Assignments for observed vibronic bands of the $\tilde{A}\leftarrow\tilde{X}$ transition of C_6H_5O in the 7650–8750 cm^{-1} region. The experimental shifts from the origin band (0_0^0) are compared with those calculated quantum-chemically.

Assignment	Band type	Obs. (cm^{-1})	Expt. shift (cm^{-1})	Calc. shift (cm^{-1})
0_0^0	*c*	7681±1	0	0
20_1^1	*c*	7732±1	51	38
14_0^1	*a*	8098±1	ν_{14}=417	416
$14_0^1 20_1^1$	*a*	8148±1	467	454
19_0^1	*b*	8180±4	ν_{19}=499	496
$14_0^1 20_2^2$	*a*	8199±2	518	492
18_0^1	*b*	8361±1	ν_{18}=680	673
17_0^1	*b*	8404±1	ν_{17}=723	710
$17_0^1 20_1^1$	*b*	8451±2	770	748
13_0^1	*a*	8474±5	ν_{13}=793	799
$17_0^1 20_2^2$	*b*	8500±3	819	786
16_0^1	*b*	8547±2	ν_{16}=866	861
$16_0^1 20_1^1$	*b*	8595±10	914	899
12_0^1	*a*	8628±1	ν_{12}=947	941
15_0^1	*b*	8645±4	ν_{15}=964	955
$12_0^1 20_1^1$	*a*	8678±3	997	979
$15_0^1 20_1^1$	*b*	8694±4	977	993
$12_0^1 20_2^2$	*a*	8728±3	1047	1017
$15_0^1 20_2^2$	*b*	8744±4	1028	1031

were also observed for other vibrational modes with a similar spacing and relative intensity, as discussed in following paragraphs.

The next intense *a*-type band was observed at 8628±1 cm^{-1}; hot bands involving transitions 20_1^1 and 20_2^2 were observed at 8678±3 and 8728±3 cm^{-1}, respectively [Fig. 2(D)]. Observed *a*-type bands at 8098 and 8628 cm^{-1} may be tentatively assigned to 14_0^1 and 12_0^1, respectively, because the separation between these two *a*-type bands, 530 cm^{-1}, is close to the difference in quantum chemically calculated vibrational wavenumbers of ν_{14}=416 cm^{-1} and ν_{12}=941 cm^{-1}. The bands at 8678 and 8728 cm^{-1} are assigned as hot bands $12_0^1 20_1^1$ and $12_0^1 20_2^2$, respectively.

The remaining *a*-type band 13_0^1, expected to lie ~8098+799−416=8481 cm^{-1}, is partially overlapped with other *b*-type bands, but observed contour suggests that this *a*-type band might lie near 8474±5 cm^{-1} [Fig. 2(C)].

The four prominent *b*-type bands lie at 8361±1, 8404±1, 8451±2, and 8500±3 cm^{-1} [Fig. 2(C)]. The separation of ~48 cm^{-1} for the last three bands also indicates that bands at 8451 and 8500 cm^{-1} are hot bands involving transitions 20_1^1 and 20_2^2, respectively, whereas the bands at 8361±1 and 8404±1 cm^{-1} are associated with two separate b_1 vibrational modes. The intensity of the band at 8404 cm^{-1}, which is greater than that of the band at 8361 cm^{-1}, also supports that the former is not a hot band of the latter transition. The six b_1 vibrational wavenumbers, $\nu_{15}-\nu_{20}$, were predicted to be 955, 861, 710, 673, 496, and 219 cm^{-1}, respectively (Table III). The separation of these two *b*-type bands, 43 cm^{-1}, is close to the difference in vibrational wavenumbers of ν_{18}=673 cm^{-1} and ν_{17}=710 cm^{-1}. The separations of these bands from the tentatively assigned 14_0^1 band at 8098, 306 and 263 cm^{-1}, respec-

tively, are also close to the quantum-chemically predicted differences of 294 and 257 cm^{-1} in harmonic vibrational wavenumbers. Hence the observed *b*-type bands at 8361 and 8404 cm^{-1} may be tentatively assigned to 18_0^1 and 17_0^1, respectively. The bands at 8451 and 8500 cm^{-1} are assigned as $17_0^1 20_1^1$ and $17_0^1 20_2^2$, respectively.

Additional *b*-type bands were observed at 8547 ± 2 and 8595 ± 10 cm^{-1} [Fig. 2(D)]; the latter is a hot band involving 20_1^1. Following a similar argument, the bands at 8547 and 8595 cm^{-1} are tentatively assigned as 16_0^1 and $16_0^1 20_1^1$, respectively, because the vibrational wavenumber of 866 cm^{-1} for the former is close to the predicted value of $\nu_{16} = 861$ cm^{-1}.

These five tentatively assigned bands of 14_0^1 at 8098 cm^{-1}, 12_0^1 at 8628 cm^{-1}, 18_0^1 at 8361 cm^{-1}, 17_0^1 at 8404 cm^{-1}, and 16_0^1 at 8547 cm^{-1} imply a band origin at 7682, 7687, 7688, 7694, and 7686 cm^{-1}, respectively; the average value of 7688 ± 4 cm^{-1} shows a standard deviation within expected error of predicted vibrational wavenumbers. Based on the predicted origin of electronic transition at 7688 ± 4 cm^{-1}, we performed a careful search near this region and observed a weak narrow line at 7681 ± 1 cm^{-1} showing a *c*-type contour [Fig. 2(A)]. Consideration of possible hot bands with *c*-type contours, such as $19_1^0 20_0^1$, does not yield satisfactory assignment for this band; hence we tentatively assign this band at 7681 cm^{-1} to the origin of the $\tilde{A} \leftarrow \tilde{X}$ transition. It is unclear how this band derives its intensity. The possibility of this band being induced by magnetic dipole transition or Coriolis-induced transition may be ruled out because an extremely weak *a*-type band is expected from such a mechanism. Based on the assignment of $\nu_0 = 7681$ cm^{-1} for C_6H_5O, we derived $\nu_{12} = 947 \pm 2$ cm^{-1}, $\nu_{13} = 793 \pm 6$ cm^{-1}, $\nu_{14} = 417 \pm 2$ cm^{-1}, $\nu_{16} = 866 \pm 3$ cm^{-1}, $\nu_{17} = 723 \pm 2$ cm^{-1}, and $\nu_{18} = 680 \pm 2$ cm^{-1}.

The *P* branches of the $15_0^1 20_n^n$ $(n=0-2)$ series *b*-type bands overlapped with the *R* branches of the $12_0^1 20_n^n$ $(n=0-2)$ series; hence the overlapped regions appear to have more intensity than expected [Fig. 2(D)]. We were able to derive bands at 8645 ± 4, 8694 ± 4, and 8744 ± 4 cm^{-1} by curve fitting and assign them to 15_0^1, $15_0^1 20_1^1$, and $15_0^1 20_2^2$, respectively. The observed vibrational wavenumber of 964 ± 4 cm^{-1} is consistent with the predicted value of $\nu_{15} = 955$ cm^{-1}.

Another *b*-type band, 19_0^1, expected to lie near $7681 + 496 = 8177$ cm^{-1}, might be attributed to the weak band near 8180 ± 4 cm^{-1} that overlapped with the $14_0^1 20_2^2$ band near 8199 cm^{-1}. The last *b*-type band, 20_0^1, is expected to lie near $7681 + 219 = 7900$ cm^{-1}. We did not observe this band, presumably due to poor Frank–Condon overlap and poor signal-to-noise ratio in this region.

We present in Fig. 3 an overview spectrum of the $\tilde{A} \leftarrow \tilde{X}$ transition of C_6H_5O [panel (A)], and stick diagrams showing tentatively assigned vibronic bands excluding hot bands [top of panel (B)] and predicted vibrational energy levels of the $\tilde{A}$ state and their band types [bottom of panel (B)] for comparison; the band types are represented with different line types. Ignoring the weak origin band, we varied the calculated wavenumbers relative to experimental values

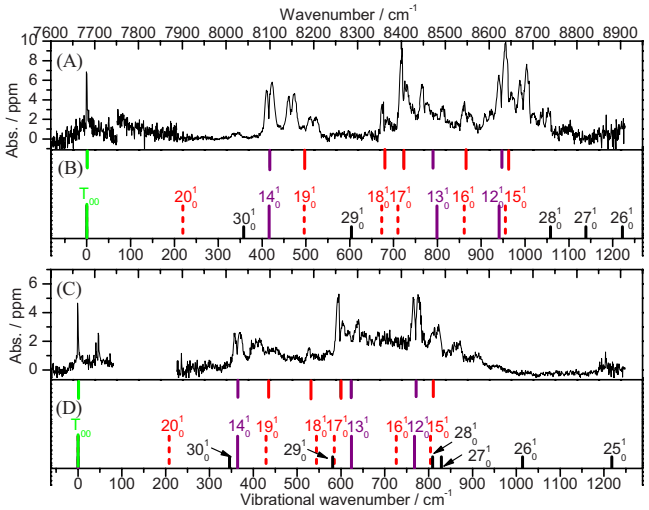

FIG. 3. (Color online) Comparison of experimental spectrum and calculated stick spectrum of C_6H_5O [panels (A) and (B)] and C_6D_5O [panels (C) and (D)] in the region 7660–8900 cm^{-1}. The stick spectra on top are experimental data and those at the bottom are harmonic vibrational wavenumbers, predicted with the B3LYP/aug-cc-pVTZ method, built upon the experimental transition origin at 7681 cm^{-1} of C_6H_5O (7661 cm^{-1} for C_6D_5O); *a*-, *b*-, and *c*-type bands are indicated with solid, dashed, and short solid lines, respectively.

to obtain the best overall match and concluded that the only satisfactory match is to assign the aforementioned *a*-type bands at 8098 and 8629 cm^{-1} to 14_0^1 and 12_0^1, respectively, as indicated in Fig. 3(B). All *a*-type and *b*-type bands except 20_0^1 were observed.

The intensity borrowing of *a*-type and *b*-type bands requires interaction of the $\tilde{A}$ state with nearby B_1 and A_2 electronic states, respectively. The $\tilde{X}\ ^2B_1$, $\tilde{B}\ ^2A_2$, and $\tilde{C}\ ^2B_1$ states might just serve the purpose. The absence of *c*-type bands, for transitions to vibrational modes $\nu_{21}-\nu_{30}$ of the $\tilde{A}$ state with b_2 symmetry, may be explained by the absence of a nearby A_1 electronic state. The $^2A_1$ state was predicted to have a vertical excitation ~4.88 eV (39 400 cm^{-1}) above the ground state;[31] it might correspond to the absorption band in the region 270–300 nm, but whether the symmetry of the upper state is A_1 or A_2 remains to be determined.[5,6,21,23,25,27–29]

The wavenumbers of the observed band origins, their assignments, and the associated vibrational wavenumbers are summarized in Table IV; the latter are also compared with scaled harmonic vibrational wavenumbers calculated quantum-chemically in Table III. All observed vibrational wavenumbers agree with the calculations to less than 4.4% (without scaling) and 1.8% (with scaling).

One would expect to observe vibrational progressions associated with the CO stretching mode of C_6H_5O because the $\tilde{A} \leftarrow \tilde{X}$ electronic transition involves a substantial change in the length of a CO bond. However, the CO stretching (ν_6) mode at 1202 cm^{-1} has an a_1 symmetry and is vibronically forbidden. Combination bands associated with ν_6 are likely to be observed, but they are outside of our range of detection.

B. Vibronic bands of C_6D_5O

Upper traces in panels (A)–(D) of Fig. 4 present the observed difference spectra in the region 7600–8620 cm^{-1}

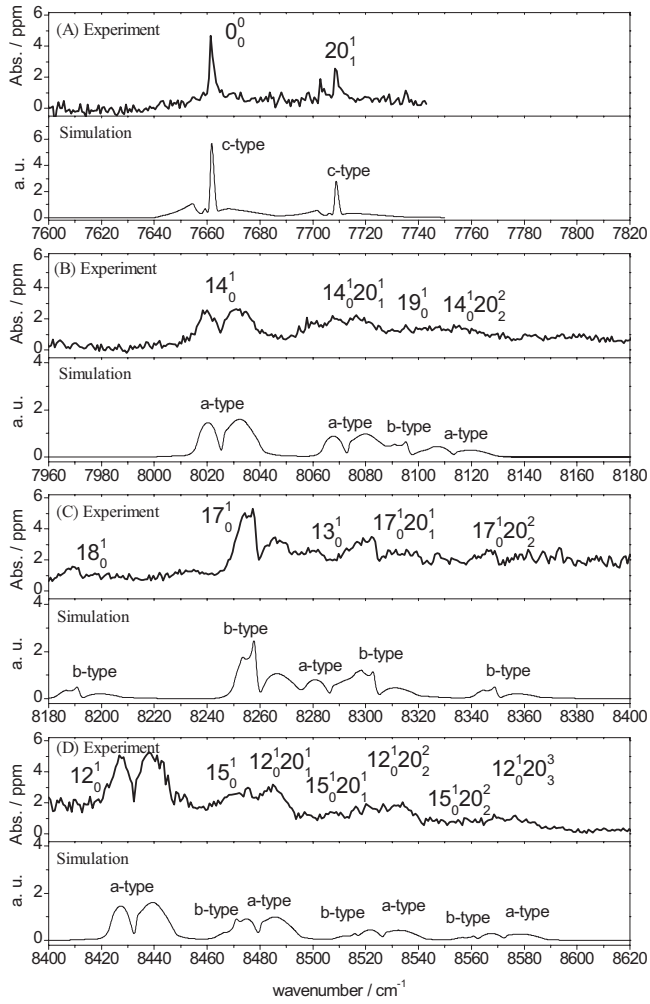

FIG. 4. Comparison of experimental spectra and simulated spectra of C_6D_5O in the region 7600–8620 cm^{-1}. The notation of the assignments is described in the text.

(1.16–1.32 μm) upon photolysis of a flowing mixture of $C_6D_5OCD_3/N_2$ (1/72, 220 Torr). Observed bands were fitted with calculated rotational parameters of C_6D_5O listed in Table I, $J_{max}=200$, $T=330$ K, and width $=1.0$ cm^{-1} using the PGOPHER program[49] to derive the band origins, as listed in Table V. Simulated spectra thus obtained are also shown in Fig. 4 for comparison.

The weak band origin of the $\tilde{A}\leftarrow\tilde{X}$ transition is shifted from 7681 ± 1 cm^{-1} for C_6H_5O to 7661 ± 1 cm^{-1} for C_6D_5O [Fig. 4(A)]. The shift of -20 cm^{-1} is consistent with the quantum-chemical predictions of -15 cm^{-1} based on the scaled harmonic vibrational wavenumbers calculated with B3LYP/aug-cc-pVTZ.[31] The *a*-type 14_0^1 band of C_6D_5O shifted from that of C_6H_5O toward smaller wavenumbers by ~72 cm^{-1}; bands at 8026 ± 1, 8074 ± 2, and 8114 ± 5 cm^{-1} are assigned to 14_0^1 and its associated hot bands $14_0^120_n^n$ ($n=1,2$) of C_6D_5O [Fig. 4(B)]. The spacing of ~50 cm^{-1} for these *a*-type bands of C_6H_5O decreases slightly to 44 ± 4 cm^{-1} for C_6D_5O; the latter separation agrees satisfactorily with the calculated energy difference between $\nu_{20}=208$ cm^{-1} of the $\tilde{A}$ state and $\nu_{20}=171$ cm^{-1} of the $\tilde{X}$ state. We thus derived $\nu_{14}=365$ cm^{-1} for C_6D_5O, consistent with the harmonic vibrational wavenumber of $\nu_{14}=364$ cm^{-1} predicted quantum chemically. The experimental isotopic ratio of $365/417=0.875$ for C_6D_5O/C_6H_5O is nearly identical to the ratio of $364/416=0.875$ derived from the scaled harmonic vibrational wavenumbers. These bands are not as well resolved as those of C_6H_5O, indicating that an additional band near 8097 ± 4 cm^{-1}, 436 cm^{-1} above the origin, and its associated hot bands might overlap with these bands. According to quantum-chemical calculations, the only b_1 vibrational mode that has vibrational wavenumbers ~436 cm^{-1} is ν_{19} (429 cm^{-1}). We thus tentatively assign this band at 8097 ± 4 cm^{-1} to 19_0^1 of C_6D_5O. The isotopic ratio of $436/499=0.874$ for 19_0^1 is close to the ratio of $429/496=0.865$ from the scaled harmonic vibrational wavenumbers.

TABLE V. Assignments for the observed vibronic bands in the 7650–8600 cm^{-1} region for the $\tilde{A}\leftarrow\tilde{X}$ transition of C_6D_5O. The experimental shifts from the origin band (0_0^0) are compared with those calculated quantum chemically.

Assignment	Band type	Obs. (cm^{-1})	Expt. shift (cm^{-1})	Calc. shift (cm^{-1})
0_0^0	*c*	7661 ± 1	0	0
20_1^1	*c*	7710 ± 1	49	37
14_0^1	*a*	8026 ± 1	$\nu_{14}=365$	364
$14_0^120_1^1$	*a*	8074 ± 2	413	401
19_0^1	*b*	8097 ± 4	$\nu_{19}=436$	429
$14_0^120_2^2$	*a*	8114 ± 5	453	438
18_0^1	*b*	8193 ± 1	$\nu_{18}=532$	544
17_0^1	*b*	8260 ± 1	$\nu_{17}=599$	585
$17_0^120_1^1$	*b*	8305 ± 1	644	622
13_0^1	*a*	8287 ± 2	$\nu_{13}=626$	624
$17_0^120_2^2$		8351 ± 5	700	659
15_0^1	*b*	8473 ± 6	$\nu_{15}=812$	804
12_0^1	*a*	8433 ± 1	$\nu_{12}=772$	768
$15_0^120_1^1$	*b*	8518 ± 3	857	841
$12_0^120_1^1$	*a*	8480 ± 2	819	805
$15_0^120_2^2$	*b*	8560 ± 8	899	878
$12_0^120_2^2$	*a*	8527 ± 5	866	842
$12_0^120_3^3$	*a*	8573 ± 8	912	879

The second *a*-type band at 8630 ± 1 cm^{-1}, 12_0^1 of C_6H_5O, shifted to 8433 ± 1 cm^{-1} for C_6D_5O; hot bands of $12_0^120_1^1$, $12_0^120_2^2$, and $12_0^120_3^3$ were observed at 8480 ± 2, 8527 ± 5, and 8573 ± 8 cm^{-1}, respectively [Fig. 4(D)]. The value of $\nu_{12}=772$ cm^{-1} implies an isotopic ratio of $772/947=0.815$, which agrees with the ratio of $768/941=0.816$ calculated from the scaled harmonic vibrational wavenumbers for ν_{12} of C_6D_5O/C_6H_5O. The *b*-type $15_0^120_n^n$ ($n=0-2$) series of C_6D_5O overlapped with the $12_0^120_n^n$ series, with the 15_0^1 band separated from the 12_0^1 by ~36 cm^{-1}, according to calculated harmonic vibrational wavenumbers; this separation is close to the separation from the hot band involving 20_1^1. With spectral simulation, we were able to locate the 15_0^1 band at 8473 ± 6 cm^{-1}, yielding $\nu_{15}=812$ cm^{-1}, similar to the predicted value of 804 cm^{-1}. The isotopic ratio of $812/964=0.842$ for 15_0^1 is nearly identical to the ratio of $804/955=0.842$ from the scaled harmonic vibrational wavenumbers. The 16_0^1 band was predicted to have wavenumbers ~42 cm^{-1} smaller than that of the 12_0^1 band, but we were unable to provide a positive identification of this band.

According to calculations, the third *a*-type band is expected to lie near $7661+624=8285$ cm^{-1}. In this region a band near 8287 ± 2 cm^{-1} was observed to lie between two *b*-type bands (assigned as 17_0^1 and $17_0^120_1^1$ in the next paragraph). We thus tentatively assign this band to 13_0^1 of C_6D_5O. The 13_0^1 band of C_6H_5O was estimated to lie $\sim8474\pm5$ cm^{-1}, 793 ± 6 cm^{-1} from the origin. The corresponding experimental isotopic ratio of $626/793=0.789$ agrees with the ratio of $624/799=0.781$ calculated from the scaled harmonic vibrational wavenumbers.

The *b*-type bands 18_0^1, 17_0^1, and $17_0^120_1^1$ of C_6D_5O were readily identified at 8193 ± 1, 8260 ± 1, and 8305 ± 1 cm^{-1}, respectively [Fig. 4(C)]. Hence $\nu_{18}=532$ cm^{-1} and $\nu_{17}=599$ cm^{-1} for C_6D_5O, consistent with the values of $\nu_{18}=544$ cm^{-1} and $\nu_{17}=585$ cm^{-1} from the calculations. The corresponding experimental isotopic ratios of $532/680=0.782$ and $599/723=0.828$ agree with the ratios of $544/673=0.808$ and $585/710=0.824$ calculated from the harmonic vibrational wavenumbers (Table III).

We also presented in Fig. 3 an overview spectrum of the $\tilde{A}\leftarrow\tilde{X}$ transition of C_6D_5O [panel (C)], and two stick diagrams showing assigned vibronic bands with hot bands excluded and predicted vibrational energy levels of the $\tilde{A}$ state and their band types [panel (D)] for comparison. The satisfactory agreement of the band type and positions between experiments and calculations provides further support for the assignments of observed bands to the $\tilde{A}\leftarrow\tilde{X}$ transition of C_6H_5O and C_6D_5O. The wavenumbers of the observed band origins, their assignments, and the associated vibrational wavenumbers of C_6D_5O are listed in Table V to compare with harmonic vibrational wavenumbers calculated quantum chemically. All observed vibrational wavenumbers agree with calculations to within 2.4%.

C. Electronic transition energy and the transition origin

High-level calculations predicted the origin to be 7242 and 8339 cm^{-1} at the B3LYP/aug-cc-pVTZ and CASPT2(9,8)/aug-cc-pVTZ level of theory. Experimentally observed origin of the $\tilde{A}\leftarrow\tilde{X}$ transition of C_6H_5O at 7681 cm^{-1} deviates from these values by 439 and −658 cm^{-1}, respectively, but is close to their average value (Table II). The ν_0 value of 7323 cm^{-1} predicted with B3LYP/aug-cc-pVTZ is the closest to our experimental value.

The value of 8550 cm^{-1} reported from photoelectron experiments[30] corresponds approximately to the average value of the two most prominent bands, 17_0^1 at 8404 cm^{-1} and 12_0^1 at 8629 cm^{-1}; an unresolved broadband spectrum in this region would show a peak near 8530 cm^{-1}. This value is also consistent with the vertical excitation energy of 8548 cm^{-1} predicted with the B3LYP/aug-cc-pVTZ method, but much smaller than a value of 9952 cm^{-1} predicted with the CASPT2(9,8)/aug-cc-pVTZ method. It is unclear why the matrix experiment[25] yielded a band at 8900 cm^{-1} as it is outside our detection region.

Observation of the origin band of the symmetry-forbidden $\tilde{A}\,^2B_2\leftarrow\tilde{X}\,^2B_1$ transition at 7681 and 7661 cm^{-1} for C_6H_5O and C_6D_5O, respectively, is unexpected. Although we could not positively rule out the possibility that these bands are due to impurity bands, we favor our present tentative assignments because these bands were observed for both C_6H_5O and C_6D_5O, with a deuterium isotopic shift of −20 cm^{-1} close to the value of −15 cm^{-1} predicted from quantum-chemical calculations. However, it should be noted that if the observed *c*-type band for the origin is true, it implies that the electronic transition (direct product of $\tilde{A}\,^2B_2\leftarrow\tilde{X}\,^2B_1$) might have a relatively strong b_1 character. Consequently the original *a*-type band (excitation to the a_2 vibrational mode of the $\tilde{A}$ state) would have some *b*-type character, the *b*-type band (excitation to the b_1 vibrational mode of the $\tilde{A}$ state) would have some *a*-type character, the originally forbidden transitions to the a_1 vibrational modes of the $\tilde{A}$ state would have some *c*-type character, and excitation to the b_2 vibrational modes of the $\tilde{A}$ state might diminish in intensity. Our observation of no band associated with excitation to b_2 vibrational modes of the $\tilde{A}$ state is consistent with such a scheme, but the mixing between *a*-type and *b*-type bands are not obvious, and no *c*-type bands associated with 9_0^1, 10_0^1, and 11_0^1 (expected near 8641, 8482, and 8185 cm^{-1}) can be positively identified, even though they might be hidden among other bands. Further theoretical and experimental investigations, such as high resolution spectroscopy, are desired to decipher this problem.

V. CONCLUSION

We have recorded in the region 1.14–1.31 μm several rovibronic bands of normal and perdeuterated phenoxy radicals in their $\tilde{A}\leftarrow\tilde{X}$ transitions with the cavity ringdown technique. For the $\tilde{A}\,^2B_2$ state, vibrational wavenumbers (in cm^{-1}) of $\nu_{12}=947$, $\nu_{13}=793$, $\nu_{14}=417$, $\nu_{15}=964$, $\nu_{16}=866$, $\nu_{17}=723$, $\nu_{18}=680$, and $\nu_{19}=499$ for C_6H_5O, and $\nu_{12}=772$, $\nu_{13}=626$, $\nu_{14}=365$, $\nu_{15}=812$, $\nu_{17}=599$, $\nu_{18}=532$, and $\nu_{19}=436$ for C_6D_5O were determined. Transitions from vibrationally excited levels of ν_{20} in the $\tilde{X}$ state were also observed; ν_{20} of the $\tilde{A}$ state is greater by 50 cm^{-1} than the $\tilde{X}$ state. These experimental results are all in agreement with the quantum-chemical predictions using B3LYP/aug-cc-pVTZ. A weak origin at 7681 cm^{-1} for the $\tilde{A}\leftarrow\tilde{X}$ transition of C_6H_5O (7661 cm^{-1} for C_6D_5O) with a *c*-type contour was observed. Quantum-chemically calculated $\tilde{A}\leftarrow\tilde{X}$ electronic transition energies using various methods deviate from experiments; the closest value, 7323 cm^{-1} with a deviation of ~5%, was derived with the B3LYP/aug-cc-pVDZ method.

Note added in proof. Our recent MRCI/aug-cc-pVTZ calculations of the 0-0 adiabatic $A\leftarrow X$ excitation energy of C_6H_5O yielded a value of 7243 cm^{-1}, similar to the B3LYP value reported in Ref. 31

ACKNOWLEDGMENTS

We thank C. Western for providing the PGOPHER spectral simulation program, the National Center for High-Performance Computing of Taiwan for computer facilities, and the National Science Council of Taiwan (Grant Nos.

NSC96-2113-M-009-025 and NSC96-2113-M-009-022) and the ATU project of the Ministry of Education, Taiwan for support.

[1] D. S. Haynes, in *Fossil Fuel Combustion*, edited by W. Bartok and A. F. Sarofim (Wiley, New York, 1991), p. 261.
[2] H. Bockhorn, *Soot Formation in Combustion* (Springer-Verlag, New York, 1995).
[3] C. Y. Lin and M. C. Lin, J. Phys. Chem. **90**, 425 (1986).
[4] R. G. W. Norrish and G. W. Taylor, Proc. R. Soc. London, Ser. A **234**, 160 (1956).
[5] F. Berho and R. Lesclaux, Chem. Phys. Lett. **279**, 289 (1997).
[6] J. Platz, O. J. Nielsen, T. J. Wallington, J. C. Ball, M. D. Hurley, A. M. Straccia, W. F. Schneider, and J. Sehested, J. Phys. Chem. A **102**, 7964 (1998).
[7] Z. Tao and Z. Li, Int. J. Chem. Kinet. **31**, 65 (1999).
[8] T. Yu, A. M. Mebel, and M. C. Lin, J. Phys. Org. Chem. **8**, 47 (1995).
[9] K. Tonokura, T. Ogura, and M. Koshi, J. Phys. Chem. A **108**, 7801 (2004).
[10] T. J. Stone and W. A. Waters, Proc. Chem. Soc., London **1962**, 253.
[11] W. T. Dixon and R. O. C. Norman, Proc. Chem. Soc., London **1963**, 97.
[12] T. J. Stone and W. A. Waters, J. Chem. Soc. **1964**, 213.
[13] W. T. Dixon and R. O. C. Norman, J. Chem. Soc. **1964**, 4857.
[14] P. Neta and R. W. Fessenden, J. Phys. Chem. **78**, 523 (1974).
[15] W. T. Dixon and D. Murphy, J. Chem. Soc., Faraday Trans. 2 **72**, 1221 (1976).
[16] A. Mukherjee, M. L. McGlashen, and T. G. Spiro, J. Phys. Chem. **99**, 4912 (1995).
[17] G. R. Johnson, M. Ludwig, and S. A. Asher, J. Am. Chem. Soc. **108**, 905 (1986).
[18] S. M. Beck and L. E. Brus, J. Chem. Phys. **76**, 4700 (1982).
[19] G. N. R. Tripathi and R. H. Schuler, J. Chem. Phys. **81**, 113 (1984).
[20] G. N. R. Tripathi and R. H. Schuler, J. Phys. Chem. **92**, 5129 (1988).
[21] J. Spanget-Larsen, M. Gil, A. Gorski, D. M. Blake, J. Waluk, and J. G. Radziszewski, J. Am. Chem. Soc. **123**, 11253 (2001).
[22] D. Pullin and L. Andrews, J. Mol. Struct. **95**, 181 (1982).
[23] B. Ward, Spectrochim. Acta, Part A **24**, 813 (1968).
[24] L. J. Johnston, N. Mathivanan, F. Negri, W. Siebrand, and F. Zerbetto, Can. J. Chem. **71**, 1655 (1993).
[25] J. G. Radziszewski, M. Gile, A. Gorski, J. Spanget-Larsen, J. Waluk, and B. J. Mroz, J. Chem. Phys. **115**, 9733 (2001).
[26] K. Kesper, F. Diehl, J. G. G. Simon, H. Specht, and A. Schweig, Chem. Phys. **153**, 511 (1991).
[27] G. Porter and F. J. Wright, Trans. Faraday Soc. **51**, 1469 (1955).
[28] F. Bayrakceken, S. Aktas, M. Toptan, and A. Unlugedik, Spectrochim. Acta, Part A **59**, 135 (2003).
[29] Y. Kajii, K. Obi, N. Nakashima, and K. Yoshima, J. Chem. Phys. **87**, 5059 (1987).
[30] R. F. Gunion, M. K. Gilles, M. L. Polak, and W. C. Lineberger, Int. J. Mass Spectrom. Ion Process. **117**, 601 (1992).
[31] C.-W. Cheng, Y.-P. Lee, and H. A. Witek, J. Phys. Chem. A **112**, 2648 (2008).
[32] D. M. Chipman, R. Liu, X. Zhou, and P. Pulay, J. Chem. Phys. **100**, 5023 (1994).
[33] J. Takahashi, T. Momose, and T. Shida, Bull. Chem. Soc. Jpn. **67**, 964 (1994).
[34] R. Liu, K. Morokuma, A. M. Mebel, and M. C. Lin, J. Phys. Chem. **100**, 9314 (1996).
[35] *NIST Computational Chemistry Comparison and Benchmark Database*, NIST Standard Reference Database No. 101, edited by R. D. Johnson III (National Institute of Standards and Technology, Gaithersburg, 2005), http://srdata.nist.gov/cccbdb.
[36] S. Hirata and M. Head-Gordon, Chem. Phys. Lett. **302**, 375 (1999).
[37] C. Adamo and V. Barone, Chem. Phys. Lett. **314**, 152 (1999).
[38] Z. Rinkevicius, I. Tunell, P. Sauek, O. Vahtras, and H. Ågren, J. Chem. Phys. **119**, 34 (2003).
[39] H. M. Chang, H. H. Jaffe, and C. A. Masmanidis, J. Phys. Chem. **79**, 1118 (1975).
[40] M. Dierksen and S. Grimme, J. Chem. Phys. **120**, 3544 (2004).
[41] C.-Y. Chung, C.-W. Cheng, Y.-P. Lee, H.-Y. Liao, E. N. Sharp, P. Rupper, and T. A. Miller, J. Chem. Phys. **127**, 044311 (2007).
[42] K. W. Busch and M. A. Busch, *Cavity-Ringdown Spectroscopy: An Ultratrace-Absorption Measurement Technique* (American Chemical Society, Washington, DC, 1999).
[43] C.-Y. Chung, J. F. Ogilvie, and Y.-P. Lee, J. Phys. Chem. A **109**, 7854 (2005).
[44] L. S. Rothman, C. P. Rinsland, A. Goldman, S. T. Massie, D. P. Edwards, J.-M. Flaud, A. Perrin, C. Camy-Peyret, V. Dana, J.-Y. Mandin, J. Schroeder, A. McCann, R. R. Gamache, R. B. Wattson, K. Yoshino, K. V. Chance, K. W. Jucks, L. R. Brown, V. Nemtchinov, and P. Varanasi, J. Quant. Spectrosc. Radiat. Transf. **60**, 665 (1998).
[45] G. Herzberg, *Molecular Spectra and Molecular Structure*, Infrared and Raman Spectra of Polyatomic Molecules, Vol. II (Krieger, Malabar, 1991).
[46] J. G. Radziszewski, Chem. Phys. Lett. **301**, 565 (1999).
[47] S. M. Mattar, J. Phys. Chem. A **111**, 251 (2007).
[48] G. Herzberg and E. Teller, Z. Phys. Chem. Abt. B **21**, 410 (1933).
[49] C. M. Western, PGOPHER, a program for simulating rotational structure, University of Bristol, http://pgopher.chm.bris.ac.uk.